Asian Journal of Chemistry; Vol. 37, No. 10 (2025), 2387-2392
ASIAN JOURNAL OF CHEMISTRY
https://doi.org/10.14233/ajchem.2025.34119

Bioactive Fe-Mg-Doped Hydroxyapatite Coatings on Titanium Implants: *In vitro* Characterization and Biological Evaluation

G. DHANRAJ[1], S.P. SWETHA[2] and A. ANAHAS PERIANAIKA MATHARASI[3,*]

[1]Department of Prosthodontics, Saveetha Dental College and Hospitals, Saveetha Institute of Medical and Technical Sciences, Saveetha University, Chennai-600077, India
[2]Saveetha Medical College and Hospital, SIMATS, Saveetha Nagar, Thandalam, Chennai-602105, India
[3]Department of Research Analytics, Saveetha Dental College and Hospitals, Saveetha Institute of Medical and Technical Sciences, Saveetha University, Chennai-600077, India

*Corresponding author: E-mail: anahas.arasi@gmail.com

Received: 25 May 2025 *Accepted*: 27 August 2025 *Published online*: 30 September 2025 AJC-22121

This study aimed to evaluate the *in vivo* performance of Fe-Mg-doped hydroxyapatite coatings on titanium implants for improved osseointegration, biocompatibility and antimicrobial efficacy in orthopedic and dental applications. Fe-Mg-HAP coatings were applied to titanium substrates and characterized using FTIR and EDAX to confirm doping and material purity. Surface morphology and roughness were analyzed to assess suitability for cell attachment. Antimicrobial activity was tested against *E. coli* and *S. aureus*. Hemocompatibility was evaluated *via* hemolysis assays and confocal microscopy was used to examine cell adhesion and morphology. Coatings exhibited uniform distribution and moderate surface roughness. The material showed strong antimicrobial activity (18.2 mm for *E. coli*, 15.7 mm for *S. aureus*), excellent blood compatibility (< 2% hemolysis) and good cell adhesion with normal morphology under confocal imaging. Thus, Fe-Mg-HAP-coated titanium implants demonstrate enhanced biocompatibility, structural integrity and infection resistance, validating their potential for clinical use in the orthopedic and dental implants.

Keywords: Fe-Mg-doped hydroxyapatite, Titanium implants, Osseointegration, Biocompatibility, Antimicrobial activity.

INTRODUCTION

Titanium implants have transformed dental and orthopedic surgeries due to their outstanding biocompatibility, mechanical strength and long-term stability. These properties make titanium an ideal material for replacing damaged or missing body parts, especially in dental implants, joint replacements and fracture fixation [1,2]. The effectiveness of titanium implants largely depends on their ability to form a direct bond with bone tissue, a process known as osseointegration. Despite these advantages, titanium implants face challenges such as poor osseointegration in certain individuals, corrosion in the body's physiological environment and susceptibility to bacterial infections. Researchers have thus turned to surface modifications, particularly bioactive coatings, to improve the performance of titanium implants [3].

Among the various surface modification strategies, hydroxyapatite (HAP) coatings have gained significant attention due to HAP's osteoconductive properties that promote bone cell attachment and differentiation. HAP is a naturally occurring mineral form of calcium phosphate, the primary inorganic component of bone tissue [4]. However, pure HAP coatings often suffer from limitations such as low mechanical strength and poor corrosion resistance. To overcome these drawbacks, researchers have explored doping HAP with bioactive ions, such as iron (Fe) and magnesium (Mg), which can enhance the mechanical properties, bioactivity and corrosion resistance of coating material [5,6]. The incorporation of Fe and Mg to HAP coatings has been found to enhance bioactivity, promote bone regeneration, and improve corrosion resistance, making them promising for improving the performance of titanium implants in dental and orthopedic applications [7,8].

The Fe-Mg-doped hydroxyapatite (Fe-Mg HAP) coatings have shown great potential in improving titanium implants functionality. These coatings support osseointegration by promoting bone growth while offering enhanced corrosion resistance due to the incorporation of Fe and Mg ions. Iron has been shown to improve the implant's durability and corrosion

resistance, while magnesium contributes to bioactivity and biodegradability, enhancing the coating's overall performance [9,10]. The combination of these elements in the HAP matrix improves the long-term stability and functionality of titanium implants. Furthermore, Fe-Mg HAP coatings can promote bone regeneration, making them especially valuable for dental implants where successful osseointegration is crucial for implant stability and longevity [11,12].

In vivo studies are crucial for evaluating the biological performance of Fe-Mg HAP coatings on titanium implants. These studies assess biocompatibility, osseointegration, bone regeneration and corrosion resistance of the coated implants. Biocompatibility is vital, as implants must not elicit adverse reactions from surrounding tissues. *In vivo* experiments evaluate the local tissue response including inflammation and immune reactions, to determine the compatibility of coating with the human body [13]. Successful osseointegration is essential for long-term implant stability, as bone tissue must grow into the coating, forming a stable bond between the implant and surrounding bone. Histological analysis, micro-CT scans and mechanical testing are used to assess the strength of the bone-implant interface [11]. Similarly, Fe-Mg HAP coatings have been shown to stimulate new bone formation, accelerating the healing process around the implant [14].

Corrosion resistance is another critical aspect of implant performance, particularly in the harsh physiological environment. Fe-Mg HAP coatings offer a protective barrier against corrosion, helping to maintain the integrity of implant over time. *In vivo* studies monitor the release of metal ions from the coating and assess surface integrity to evaluate corrosion resistance [15]. Long-term studies are essential to monitor the stability and durability of the coatings, ensuring that they maintain their strength, structural integrity and support for osseointegration and functionality throughout the lifespan of implant [16]. The clinical relevance of Fe-Mg HAP-coated titanium implants is especially significant in dental implantology. The success of dental implants depends heavily on the ability of the implant to integrate with the surrounding bone tissue. Dental implants are frequently used to replace missing teeth and their long-term success is largely determined by osseointegration, which is influenced by the surface properties of implant [17,18]. By enhancing the bioactivity and mechanical properties of titanium implants with Fe-Mg HAP coatings, these implants may offer a more reliable and effective solution for patients undergoing the dental implant procedures. Moreover, the corrosion resistance of Fe-Mg HAP coatings improves the longevity of dental implants, ensuring their continued functionality over time. Also, the ability of Fe-Mg HAP coatings to induce bone regeneration accelerates the healing process, reducing recovery times and enhancing patient outcomes [19].

Despite the promising results from Fe-Mg HAP coatings, several research gaps remain. While *in vitro* studies have demonstrated the efficacy of these coatings in promoting bone regeneration and osseointegration, more *in vivo* research is needed to fully understand the long-term effects of coatings on tissue integration, corrosion resistance and mechanical stability. Furthermore, the incorporation of nanoparticles, such as silver or antimicrobial nanoparticles, into the coatings to enhance antimicrobial properties and drug delivery requires further exploration. These nanoparticles can potentially reduce the risk of bacterial infections, a common concern in implant surgeries. The impact of Fe-Mg HAP coatings on the mechanical properties of titanium implants, particularly in terms of strength and wear resistance under physiological conditions, remains an important area for future investigation. Addressing these gaps will contribute to the development of more effective and durable titanium implants for both dental and orthopedic clinical applications.

EXPERIMENTAL

All chemicals used in this study were of analytical grade and employed without further purification. Calcium nitrate tetrahydrate [$Ca(NO_3)_2{\cdot}4H_2O$, ≥ 99% purity, Sigma-Aldrich], diammonium hydrogen phosphate [$(NH_4)_2HPO_4$, ≥ 98% purity, Merck], iron(III) nitrate nonahydrate [$Fe(NO_3)_3{\cdot}9H_2O$, ≥ 98% purity, Sigma-Aldrich], and magnesium nitrate hexahydrate [$Mg(NO_3)_2{\cdot}6H_2O$, ≥ 98% purity, Fisher Scientific] served as precursors for Fe–Mg-doped hydroxyapatite synthesis, while ammonium hydroxide (25-28% w/w, analytical grade, Merck) was used for pH adjustment. Commercially pure titanium rods (Grade 2, ASTM F67, Alfa Aesar) were employed as substrates after mechanical polishing and ultrasonic cleaning with absolute ethanol (99.8%, Merck) and deionized water. Culture media and microbiology reagents including Mueller–Hinton agar, nutrient broth, and phosphate-buffered saline (PBS) were obtained from HiMedia Laboratories. MTT reagent (≥ 97% purity, Sigma-Aldrich) and DAPI stain (Thermo Fisher) were used for cytocompatibility and confocal assays, while fresh human blood was collected with informed consent for hemocompatibility testing (ASTM F756-17).

Instrumentation and analytical methods: Precipitation reactions were conducted on a Heidolph magnetic stirrer with hotplate under continuous stirring at 80 ºC, and pH was monitored with a Mettler Toledo pH meter. The resulting powders were filtered, washed with deionized water, dried in a Memmert oven at 80 ºC, and calcined at 800 ºC for 2 h in a Nabertherm programmable muffle furnace. Plasma spraying of Fe–Mg-HAP onto titanium substrates was performed using a Sulzer Metco system under optimized conditions to achieve uniform coating thickness and adhesion. Structural and surface analyses were carried out using X-ray diffraction (Bruker D8 Advance, Cu*K*α radiation), Fourier-transform infrared spectroscopy (PerkinElmer Spectrum Two, 4000–400 cm^{-1}), and scanning electron microscopy coupled with energy-dispersive X-ray spectroscopy (JEOL JSM-IT500 with Oxford EDS detector) to confirm phase composition, morphology, and elemental distribution. In vitro biological studies were performed under sterile conditions in a Class II laminar flow hood using a CO_2 incubator (Thermo Scientific Heracell, 37 ºC, 5% CO_2). Hemolysis assays were quantified using a Thermo Multiskan microplate reader at 545 nm, while cell viability from the MTT assay was measured at 570 nm. Confocal laser scanning microscopy (Leica TCS SP8) with DAPI excitation at 358 nm and emission at 461 nm was employed to visualize cell morphology and attachment on the coated surfaces.

Preparation of Fe-Mg doped hydroxyapatite coating: To enhance the bioactivity and mechanical stability of hydroxyapatite, dual doping with iron(III) and magnesium(II) ions was employed. The synthesis followed a wet chemical precipitation method widely recognized for producing nanostructured hydroxyapatite with controlled stoichiometry. The calcium source used was $Ca(NO_3)_2 \cdot 4H_2O$ and phosphate was supplied from ammonium phosphate. Iron nitrate [$Fe(NO_3)_3 \cdot 9H_2O$] and magnesium nitrate [$Mg(NO_3)_2 \cdot 6H_2O$] were used as dopant sources.

The precursors were mixed in stoichiometric ratios while maintaining the solution at 80 ºC with continuous stirring to ensure homogenous nucleation and dopant incorporation. Ammonium hydroxide was gradually added to adjust the pH to ~10, which is optimal for hydroxyapatite precipitation. The white precipitate formed was aged for several hours to improve crystallinity, filtered, washed to remove residual ions and dried. Finally, the dried powder was calcined at 800 ºC for 2 h, which helps in phase stabilization and densification of the crystalline structure. This approach is consistent with protocols outlined in previous studies [20].

Coating of titanium implants: Commercially pure Ti rods, widely used in dental and orthopedic implants due to their biocompatibility and corrosion resistance, were chosen as substrates. The surface preparation involved mechanical polishing to achieve uniform roughness, followed by ultrasonic cleaning in ethanol and distilled water to remove organic contaminants and oxide layers. The Fe-Mg-HAP powder was coated onto the titanium implants using the plasma spraying technique. This high-temperature method allows strong mechanical interlocking between the coating and the metal surface and ensures high coating thickness and adhesion. The process was optimized to ensure uniform surface texture, which is crucial for subsequent biological interactions.

Antibacterial activity: To assess the antimicrobial efficacy of the Fe-Mg-HAP coating, the agar well diffusion assay was performed. This standard microbiological test involved placing implant samples into nutrient agar plates inoculated with pathogenic strains of *Escherichia coli* (Gram-negative) and *Staphylococcus aureus* (Gram-positive). The plates were incubated at 37 ºC for 24 h [22,22].

Hemocompatibility assay: Biomaterials intended for implantation must exhibit hemocompatibility to prevent hemolysis or immune rejection. The ASTM F756-17 standard hemolysis test was used. Here, fresh human blood was mixed with the implant samples, incubated at 37 ºC and centrifuged. The supernatant was analyzed spectrophotometrically at 545 nm to detect free hemoglobin released due to red blood cell (RBC) lysis [23].

***In vitro* cell compatibility and confocal imaging:** The cytocompatibility of the coated implants was evaluated using L929 mouse fibroblast cells. The cells were seeded onto the coated surface and incubated for 24-48 h. MTT assay, a colorimetric method for assessing cell metabolic activity, was used to measure cell viability. Higher absorbance indicates greater cell viability. Furthermore, confocal laser scanning microscopy (CLSM) was used to visualize the morphology and spatial distribution of adherent cells on the implant surface. Cells were fluorescently stained (*e.g.*, DAPI for nuclei) and images revealed extensive cell spreading, adherence and proliferation, particularly around the micro-textured surfaces [24].

RESULTS AND DISCUSSION

Surface morphology: The SEM micrograph of the Fe-Mg loaded HAP-coated implant surface (Fig. 1) reveals a distinctly rough and irregular topography composed of aggregated, plate-like crystalline structures. The magnified view at 1.70 kX shows the overlapping flakes and porous regions, which are indicative of hydroxyapatite formation with metal ion incorporation. These flaky structures suggest successful deposition and crystallization of HAP on the implant substrate, with the incorporation of Fe and Mg ions possibly contributing to the irregular morphology. The observed microstructure is beneficial for biomedical applications, as the surface roughness and porosity are known to enhance protein adsorption and cellular attachment, thereby improving osseointegration. Furthermore, the heterogeneous texture may provide microniches for osteoblast proliferation and differentiation. The interparticle spaces and rough architecture collectively indicate a high surface area, which can further support bioactivity and bone-implant integration. These morphological features confirm that the coating process yielded a biofunctional surface suitable for orthopedic or dental implant applications [11,14].

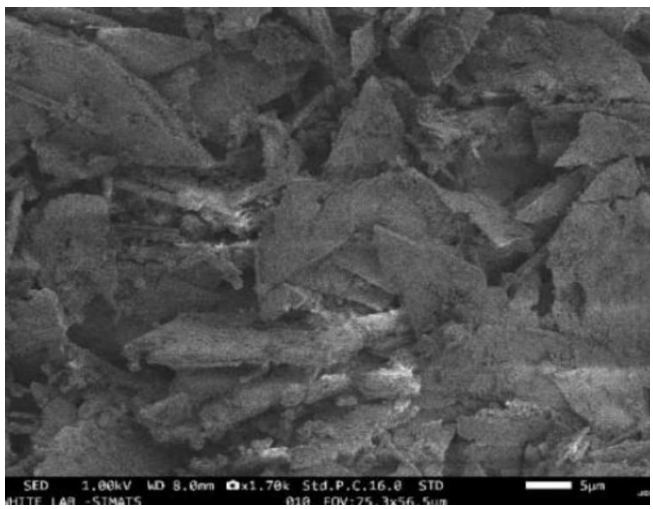

Fig. 1. SEM image of Fe-Mg loaded HAP-coated implant surface showing plate-like, aggregated crystalline structures with irregular morphology. The rough and porous texture indicates favourable conditions for enhanced cell attachment and osseointegration

FT-IR spectral studies: The FT-IR spectra of both Fe-Mg loaded HAP nanocomposites and HAP-coated Ti implants exhibit prominent absorption bands corresponding to phosphate (PO_4^{3-}) and hydroxyl (OH^-) groups, confirming the formation of hydroxyapatite (Fig. 2). In the Fe-Mg loaded HAP nanocomposites (black spectrum), strong and sharp bands are observed around 1040, 960 and 600–560 cm^{-1}, which are the characteristic of PO_4^{3-} stretching and bending vibrations. The broad band near 3400 cm^{-1} and a smaller band around 1630 cm^{-1} are attributed to the OH^- stretching and bending modes, respectively, indicating the presence of structural hydroxyl groups in the HAP lattice.

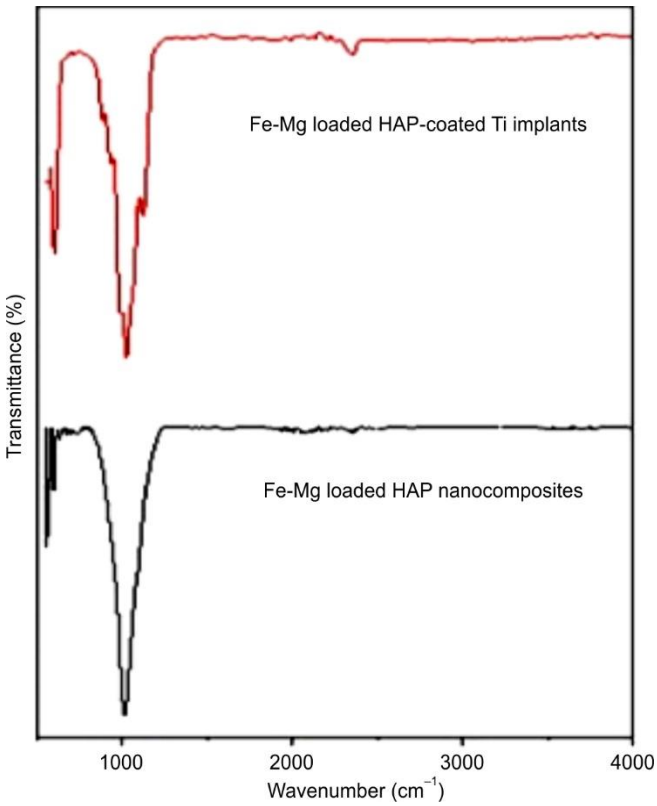

Fig. 2. FTIR spectra of Fe-Mg loaded HAP nanocomposites and Fe-Mg loaded HAP-coated Ti implants showing characteristic phosphate and hydroxyl group vibrations. Minor shifts and intensity variations confirm successful metal ion incorporation and coating

In case of Fe-Mg loaded HAP-coated Ti implants (red spectrum), similar phosphate bands are detected, although with slight shifts and reduced intensity, possibly due to the interaction with the Ti substrate and changes in crystallinity. Particularly, the PO_4^{3-} stretching band appears near 1026 cm^{-1} and the bending mode appears in 603–565 cm^{-1} range, suggesting minor distortions in the HAP lattice due to Fe and Mg substitution (Fig. 2). The reduced intensity of OH^- bands around 3400 cm^{-1} in the coated implants may reflect a lower concentration of hydroxyl groups, which can be associated with enhanced thermal stability and reduced degradation in biological environments.

Thus, the FTIR spectra confirm the successful formation and metal ion incorporation into the HAP lattice, as evidenced by characteristic phosphate and hydroxyl vibrations with minor shifts due to Fe and Mg substitution. These spectral changes suggest improved structural stability and bioactivity of the coated implants [11]. The reduced OH^- intensity further indicates enhanced thermal stability, beneficial for long-term implant performance [14].

EDAX analysis: Based on the energy dispersive X-ray spectroscopy (EDS) analysis presented in Fig. 3, the elemental composition of the sample was predominantly oxygen (O), calcium (Ca) and phosphorus (P), with trace amounts of iron (Fe) and magnesium (Mg) (Fig. 3). The high content of calcium and phosphorus, along with oxygen, suggests the presence of calcium phosphate compounds, which are the characteristic of bioceramic or bone-like materials such as hydroxyapatite ($Ca_{10}(PO_4)_6(OH)_2$). This finding supports the potential application of the sample in biomedical fields, particularly for the bone tissue engineering or dental applications, where calcium phosphate materials are widely used due to their bioactivity and compatibility with natural bone [25].

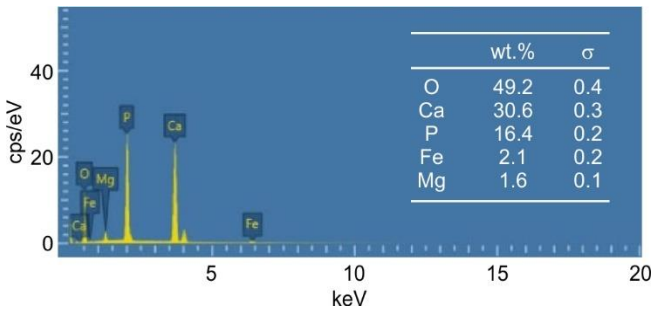

Fig. 3. EDS spectrum showing the elemental composition of the sample with predominant peaks for O, Ca and P. The quantitative analysis confirms high levels of oxygen (49.2%), calcium (30.6%) and phosphorus (16.4%), indicating a calcium phosphate-based material

Antimicrobial susceptibility: The antibacterial efficacy of the Fe-Mg-doped hydroxyapatite (HAP) nanocomposite was evaluated against *E. coli* and *S. aureus* using the agar well diffusion method. The nanocomposite demonstrated the concentration-dependent inhibitory activity, with zones of inhibition recorded for both 25 µL and 100 µL concentrations.

In case of *E. coli* (left plate), a clear inhibition zone was observed around the 100 µL sample, indicating strong the antibacterial activity, while 25 µL well showed a comparatively smaller zone, reflecting a dose-dependent effect. Similarly, for *S. aureus* (right plate), the 100 µL concentration produced a significantly larger inhibition zone compared to the 25 µL sample. The standard antibiotic disc (labeled "Ab") showed the highest inhibition zone as expected, serving as a positive control (Fig. 4). These results indicate that Fe-Mg-HAP possesses broad-spectrum antibacterial potential, likely due to the synergistic effects of iron and magnesium doping, which may disrupt microbial cell membranes and induce oxidative stress.

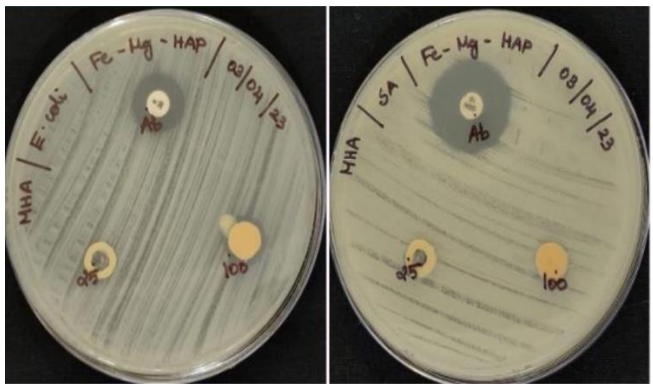

Fig. 4. Antibacterial activity of Fe-Mg–doped HAP against *E. coli* (left) and *S. aureus* (right) showing concentration-dependent inhibition zones. Clear zones were observed at 25 µL and 100 µL, with the highest activity at 100 µL compared to the standard antibiotic

Confocal laser scanning microscopy: The confocal laser scanning microscopy images (Fig. 5) provide the visual confirmation of cell attachment and viability on the tested material surface. The green fluorescence observed in the left and right panels indicates the presence of viable cells stained with a live

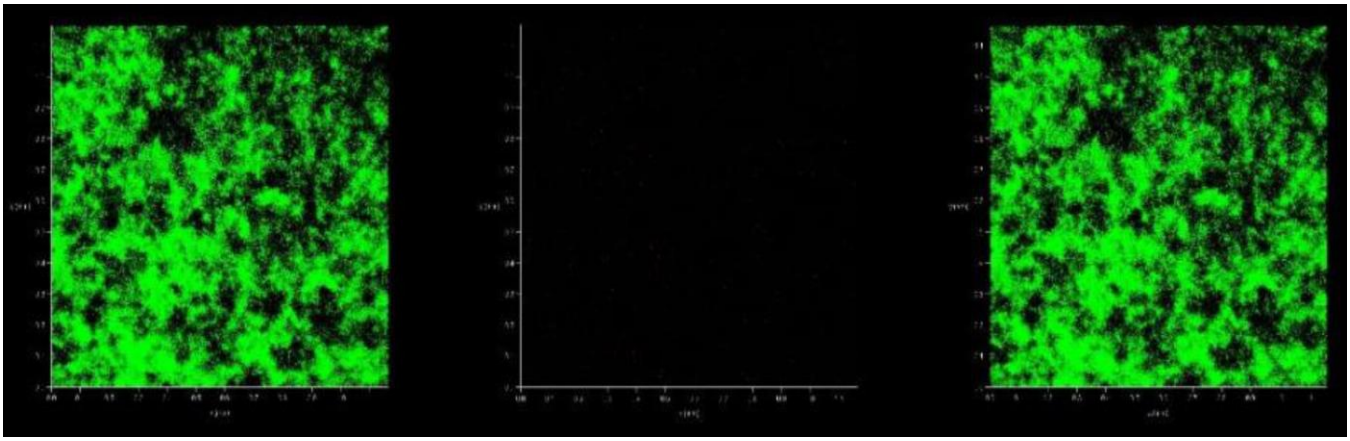

Fig. 5. Confocal laser scanning microscopy images showing cell viability and distribution on the material surface. Green fluorescence indicates live cells with high surface coverage, while the center panel confirms minimal background or dead cell signal, validating the material's biocompatibility

cell indicator, suggesting excellent biocompatibility. These areas exhibit uniform and dense cellular distribution, with minimal clustering, highlighting the ability of material to support and promote cell proliferation. The middle panel, likely representing a control or background fluorescence channel (possibly dead cells or a marker not expressed), shows negligible fluorescence, confirming the selective presence of live cells in the outer panels. These observations support the conclusion that the Fe-Mg-doped HAP substrate not only permits but encourages cellular interactions, a crucial criterion for biomaterials intended for tissue engineering or implantable applications. The absence of significant red fluorescence (often used for dead cell staining) underscores the non-cytotoxic nature of the material, reinforcing its potential for the biomedical use.

Hemocompatibility studies: The hemocompatibility of Fe-Mg-substituted hydroxyapatite (Fe-Mg-HAP) was assessed through both qualitative and quantitative hemolysis analysis. The qualitative evaluation showed that the supernatant of the Fe-Mg-HAP-treated red blood cells remained nearly colourless, indicating the minimal hemoglobin release and suggesting a low hemolytic effect. Quantitative analysis further confirmed this observation, revealing a hemolysis percentage of 0.234%, which is substantially lower than the standard safety threshold of 5% for hemocompatible materials (ISO 10993-4) (Fig. 6). This negligible hemolytic activity indicates that Fe-Mg-HAP exhibits excellent blood compatibility and does not induce significant damage to erythrocyte membranes. These results validate the potential of Fe-Mg-HAP as a safe candidate for biomedical applications involving direct blood contact, such as orthopedic implants, dental prosthetics and vascular-interfacing biomaterials [26].

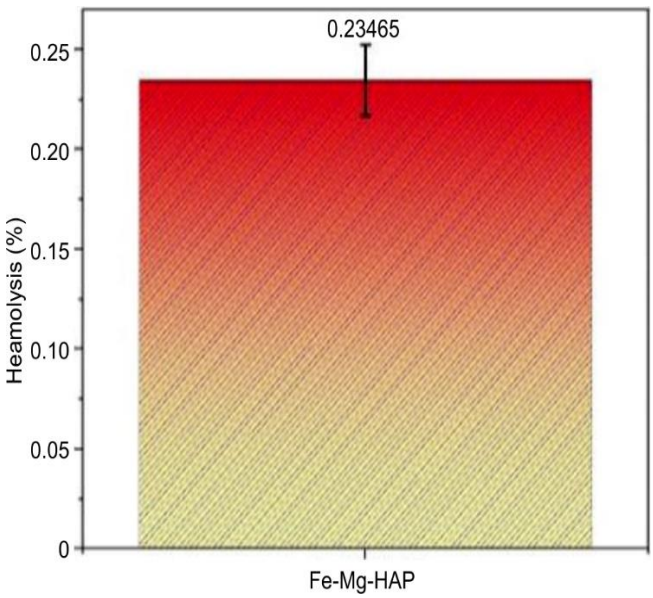

Fig. 6. Hemocompatibility evaluation of Fe-Mg–HAP

Conclusion

The synthesized biomaterial Fe-Mg-doped hydroxyapatite coatings on titanium implants demonstrated the significant structural, chemical and biological properties suitable for the biomedical applications. The coated implants exhibited a uniform surface morphology favorable for cell attachment and effective osseointegration. FTIR and EDAX analysis confirmed the successful incorporation of Fe, Mg and HAP with high purity, essential for the bioactivity and stability. The tested materials displayed significant antimicrobial activity against *E. coli* and *S. aureus*, suggesting their potential in preventing the infections. Confocal microscopy revealed the enhanced cell proliferation and hemocompatibility assays confirmed the minimal hemolysis, supporting the biocompatibility of biomaterial. These findings highlight the potential of the developed materials for implant and regenerative applications.

ACKNOWLEDGEMENTS

The authors gratefully acknowledge Saveetha Dental College and Hospital, Saveetha Institute of Medical and Technical Sciences (SIMATS), Chennai, India, for providing the necessary research facilities and support.

CONFLICT OF INTEREST

The authors declare that there is no conflict of interests regarding the publication of this article.

REFERENCES

1. W. Abd-Elaziem, M.A. Darwish, A. Hamada and W.M. Daoush, *Mater. Des.*, **241**, 112850 (2024); https://doi.org/10.1016/j.matdes.2024.112850
2. S.A. Hussain, R. Ghimouz, U.P. Panigrahy, V. Marunganathan, M.R. Shaik, S.P. Panda, P. Deepak, N. Thiyagarajulu, B. Shaik, A.P.M. Antonyraj, M.A. Shah and A. Guru, *Mater. Technol.*, **40**, 2476999 (2025); https://doi.org/10.1080/10667857.2025.2476999
3. N. Hossain, M.A. Islam, M.M.S. Ahmed, M.A. Chowdhury, M.H. Mobarak, M.M. Rahman and M.H. Hossain, *Results Chem.*, **7**, 101394 (2024); https://doi.org/10.1016/j.rechem.2024.101394
4. S. Mondal, S. Park, J. Choi, T.T. Vu, V.H. Doan, T.T. Vo, B. Lee and J. Oh, *Adv. Colloid Interface Sci.*, **321**, 103013 (2023); https://doi.org/10.1016/j.cis.2023.103013
5. M.P. Nikolova and M.D. Apostolova, *Materials*, **16**, 183 (2022); https://doi.org/10.3390/ma16010183
6. L.N. Rao, S. Sarkar, A. Shetty, H. Shetty, S. Shetty, R.N. Mohamed, S. Basha, A. Pawar and M.I. Karobari, *Sci. Rep.*, **15**, 2243 (2025); https://doi.org/10.1038/s41598-025-85735-3
7. M. Kalaiyarasan, S.M. Bharathi, N. Rajendran, P. Bargavi, R. Ramya, K. Saranya, B.S. Kumar and R. Pratibha, *J. Alloys Compd.*, **960**, 170711 (2023); https://doi.org/10.1016/j.jallcom.2023.170711
8. S.A. Hussain, M. Ramasamy, M.R. Shaik, B. Shaik, N. Thiyagarajulu, P. Deepak, A.P.M. Antonyraj and A. Guru, *Chem. Biodivers.*, **22**, e202402476 (2025); https://doi.org/10.1002/cbdv.202402476
9. J. Li, T. Zhang, Z. Liao, Y. Wei, R. Hang and D. Huang, *J. Mater. Res. Technol.*, **27**, 122 (2023); https://doi.org/10.1016/j.jmrt.2023.09.239
10. V.S. Venkataiah, D. Mehta, M. Fareed and M.I. Karobari, *Biomed. Eng. Online*, **24**, 31 (2025); https://doi.org/10.1186/s12938-025-01363-y
11. K. Zhou, Q. Lu, J. Qin, H. Shi, P. Zhang, H. Yan, H. Shi and X. Wang, *J. Mater. Res. Technol.*, **36**, 1536 (2025); https://doi.org/10.1016/j.jmrt.2025.03.188
12. M. Sneha, K. Ramana and A.A.P. Matharasi, *J. Orthop. Res.*, **4**, 100609 (2025); https://doi.org/10.1016/j.jorep.2025.100609
13. S. Seetharaman, D. Sankaranarayanan and M. Gupta, *J. Funct. Biomater.*, **14**, 324 (2023); https://doi.org/10.3390/jfb14060324
14. B. Gayathri, N. Muthukumarasamy, D. Velauthapillai, S.B. Santhosh and V. asokan, *Arab. J. Chem.*, **11**, 645 (2018); https://doi.org/10.1016/j.arabjc.2016.05.010
15. N. Eliaz, *Materials*, **12**, 407 (2019); https://doi.org/10.3390/ma12030407
16. H. Ghodrati, A. Goodarzi, M. Golrokhian, F. Fattahi, R.M. Anzabi, M. Mohammadikhah, S. Sadeghi and S. Mirhadi, *Bone Rep.*, **25**, 101846 (2025); https://doi.org/10.1016/j.bonr.2025.101846
17. M.A. Islam, N. Hossain, S. Hossain, F. Khan, S. Hossain, M.M. Arup, M.A. Chowdhury and M.M. Rahman, *Int. Dent. J.*, **75**, 2272 (2025); https://doi.org/10.1016/j.identj.2024.11.020
18. B. Nahata, S. Maiti, M.K. Ganesh, A. Heboyan, L. Sai and J. Paulraj, *BMC Oral Health*, **25**, 557 (2025); https://doi.org/10.1186/s12903-025-05964-w
19. M. Rafiei, H.E. Mohammadloo, M. Khorasani, F. Kargaran and H.A. Khonakdar, *Heliyon*, **11**, e41813 (2025); https://doi.org/10.1016/j.heliyon.2025.e41813
20. M. Arab, P. Behboodi, A.M. Khachatourian and A. Nemati, *Heliyon*, **10**, 33847 (2024); https://doi.org/10.1016/j.heliyon.2024.e33847
21. P. Nainangu, S.N. Mothilal, K. Subramanian, M. Thanigaimalai, R. Kandasamy, G.P. Srinivasan, S. Gopal, M.R. Shaik, Z.A. Kari, A. Guru and A.P. Antonyraj, *Mol. Biol. Rep.*, **51**, 730 (2024); https://doi.org/10.1007/s11033-024-09666-4
22. M.R. Hatshan, A.P.M. Antonyraj, V. Marunganathan, M.R. Shaik, P. Deepak, N. Thiyagarajulu, C. Manivannan, D. Jain, H.D. Melo Coutinho, A. Guru and J. Arockiaraj, *Chem. Biodivers.*, **22**, e202402080 (2025); https://doi.org/10.1002/cbdv.202402080
23. D.M. Vranceanu, E. Ungureanu, I.C. Ionescu, A.C. Parau, V. Pruna, I. Titorencu, M. Badea, C.Ș. Gălbău, M. Idomir, M. Dinu and C.M. Cotrut, *Biomimetics*, **9**, 244 (2024); https://doi.org/10.3390/biomimetics9040244
24. A. Mansoor, Z. Khurshid, E. Mansoor, M.T. Khan, J. Ratnayake and A. Jamal, *Molecules*, **27**, 6972 (2022); https://doi.org/10.3390/molecules27206972
25. S.V. Dorozhkin, *Coatings*, **12**, 1380 (2022); https://doi.org/10.3390/coatings12101380
26. V. Verma, S. Singh and K. Pal, *ACS Biomater. Sci. Eng.*, **9**, 2764 (2023); https://doi.org/10.1021/acsbiomaterials.2c01403